Note on the SEOBNRv5PHM waveform model

Antoni Ramos-Buades and the v5PHM team[1]

[1]*Max Planck Institute for Gravitational Physics (Albert Einstein Institute), Am Mühlenberg 1, Potsdam, 14476, Germany*

(Dated: February 9, 2023)

This note is based on one of the papers we are writing on the SEOBNRv5PHM waveform model. It summarizes the structure of the Hamiltonian, post-Newtonian spin-precessing evolution equations and explains the construction of the multipolar waveform modes of the SEOBNRv5PHM model. Please keep in mind, when reading this note, that citations are not complete. The note has been written with the only scope of facilitating the review of the SEOBNRv5PHM model for O4.

NOTATION

In this paper, we use geometric units, setting $G = c = 1$ unless otherwise specified.

We consider a binary with masses m_1 and m_2, with $m_1 \geq m_2$, and spins $\boldsymbol{S}_1$ and $\boldsymbol{S}_2$. We define the following combinations of the masses:

$$\begin{aligned} M &\equiv m_1 + m_2, \quad \mu \equiv \frac{m_1 m_2}{M}, \quad \nu \equiv \frac{\mu}{M}, \\ \delta &\equiv \frac{m_1 - m_2}{M}, \quad q \equiv \frac{m_1}{m_2}, \quad X_{\rm i} \equiv \frac{m_{\rm i}}{M}, \end{aligned} \tag{1}$$

where i = 1, 2, and define the dimensionless spin vectors

$$\boldsymbol{\chi}_{\rm i} \equiv \frac{\boldsymbol{a}_{\rm i}}{m_{\rm i}} = \frac{\boldsymbol{S}_{\rm i}}{m_{\rm i}^2}, \tag{2}$$

along with the intermediate definition for $\boldsymbol{a}_{\rm i}$, and the combinations

$$\boldsymbol{a}_{\pm} \equiv \frac{\boldsymbol{a}_1 \pm \boldsymbol{a}_2}{M} = \frac{m_1}{M}\boldsymbol{\chi}_1 \pm \frac{m_2}{M}\boldsymbol{\chi}_2. \tag{3}$$

Note that, unlike $\boldsymbol{a}_{\rm i}$, we define $\boldsymbol{a}_{\pm}$ to be dimensionless by dividing $\boldsymbol{a}_{\rm i}$ by the total mass.

The relative position and momentum vectors are denoted $\boldsymbol{R}$ and $\boldsymbol{P}$, with

$$\boldsymbol{P}^2 = P_R^2 + \frac{L^2}{R^2}, \qquad P_R = \boldsymbol{n}\cdot\boldsymbol{P}, \qquad \boldsymbol{L} = \boldsymbol{R}\times\boldsymbol{P}, \tag{4}$$

where $\boldsymbol{n} = \boldsymbol{R}/R$, and $\boldsymbol{L}$ is the orbital angular momentum with magnitude L. The total angular momentum $\boldsymbol{J} = \boldsymbol{L} + \boldsymbol{S}_1 + \boldsymbol{S}_2$.

We use the rescaled dimensionless variables

$$\begin{aligned} t \equiv \frac{T}{M}, \quad \boldsymbol{r} \equiv \frac{\boldsymbol{R}}{M}, \quad u \equiv \frac{1}{r}, \quad \tilde{\boldsymbol{L}} = \frac{\boldsymbol{L}}{M\mu}, \quad \boldsymbol{p} \equiv \frac{\boldsymbol{P}}{\mu}, \\ p_r \equiv \frac{P_R}{\mu}, \quad \tilde{\Omega} \equiv M\Omega, \quad \tilde{H} \equiv \frac{H}{\mu}, \end{aligned} \tag{5}$$

where we use either a lowercase symbol or a tilde to indicate the dimensionless quantities.

I. EFFECTIVE-ONE-BODY DYNAMICS OF SPIN-PRECESSING BINARY BLACK HOLES

The EOB formalism [1–3] provides an analytical description of the GW emission of the full coalescence process, particularly inspiral, merger and ringdown. Its accuracy can be highly increased by including information from gravitational self-force and NR. The EOB framework can also naturally accommodate the effects of spin precession [4–6] and eccentricity [7–9].

For the two-body conservative dynamics, the EOB approach relies on a Hamiltonian $H_{\rm EOB}$, constructed through the effective Hamiltonian $H_{\rm eff}$ of a nonspinning particle of mass μ moving in a deformed Kerr spacetime of mass M and spin $\boldsymbol{a}_{\rm Kerr}$ [10–12], and an energy map connecting $H_{\rm eff}$ and $H_{\rm EOB}$ [1]

$$H_{\rm EOB} = M\sqrt{1 + 2\nu\left(\frac{H_{\rm eff}}{\mu} - 1\right)}. \tag{6}$$

The deformation of the Kerr metric is fixed by imposing that at each PN order the PN-expanded EOB Hamiltonian agrees with a PN Hamiltonian in another gauge after a canonical transformation. In Ref. [12], we derived an EOB Hamiltonian that includes all generic-spin information up to 4PN, while the non-spinning dynamics is incorporated up to 4PN with partial 5PN results. The dynamical variables of the generic EOB Hamiltonian are the orbital separation $\boldsymbol{r}$, the corresponding canonically conjugate momentum $\boldsymbol{p}$, and the spins $\boldsymbol{S}_{1,2}$.

For arbitrary orientations of the spins, both the orbital plane and the spins precess around the total angular momentum of the system $\boldsymbol{J} = \boldsymbol{L} + \boldsymbol{S}_1 + \boldsymbol{S}_2$, where the orbital angular momentum $\tilde{\boldsymbol{L}} = \boldsymbol{r}\times\boldsymbol{p}$. The equations of motion are as follows

$$\begin{aligned} \dot{\boldsymbol{r}} &= \frac{\partial \tilde{H}_{\rm EOB}}{\partial \boldsymbol{p}}, \qquad \dot{\boldsymbol{p}} = -\frac{\partial \tilde{H}_{\rm EOB}}{\partial \boldsymbol{r}} + \mathcal{F}, \\ \frac{d\boldsymbol{S}_{1,2}}{dT} &= \frac{\partial H_{\rm EOB}}{\partial \boldsymbol{S}_{1,2}} \times \boldsymbol{S}_{1,2}, \end{aligned} \tag{7}$$

where the full precessing-spin Hamiltonian is given in Sec. II. D of Ref. [12], and it reduces as $\nu \to 0$ to the Kerr Hamiltonian for a test mass in a generic orbit. Within the EOB formalism, the dissipative effects enter in the dynamics through the radiation-reaction force $\mathcal{F}$, which is expressed in terms of the waveform modes [13–15].

Solving the EOB dynamics for generic spin configurations can be computationally expensive as the EOB evolution equations (7) lead to lengthy expressions [16]. Thus, to increase the efficiency of the model, we work in the co-precessing frame [17–21], in which the z-axis is aligned with the Newtonian angular momentum $\tilde{\boldsymbol{L}}_N \equiv \boldsymbol{r}\times\dot{\boldsymbol{r}}$, which is instantaneously perpendicular to the orbital plane. In that frame, one can approximate the dynamics using the non-precessing EOB evolution equations, which are expressed in terms of the orbital

separation r, orbital phase ϕ, and their canonically-conjugate momenta p_r and p_ϕ. The equations of motion read

$$\dot{r} = \xi(r)\frac{\partial \tilde{H}_{\rm EOB}}{\partial p_{r_*}}, \tag{8a}$$

$$\dot{\phi} = \frac{\partial \tilde{H}_{\rm EOB}}{\partial p_\phi}, \tag{8b}$$

$$\dot{p}_{r_*} = -\xi(r)\frac{\partial \tilde{H}_{\rm EOB}}{\partial r} + \mathcal{F}_r, \tag{8c}$$

$$\dot{p}_\phi = \mathcal{F}_\phi. \tag{8d}$$

We use a Hamiltonian that reduces, in the aligned-spin limit, to the Hamiltonian of `SEOBNRv5HM` [22], but also includes orbit-averaged precessing-spin information for circular orbits. (See Appendix III for details.)

As in previous EOB models [4, 6, 23, 24], the evolution of the radial momentum is performed using the tortoise-coordinate $p_{r_*} = p_r \xi(r)$, where $\xi(r) = dr/dr_*$. The radiation-reaction force is computed using [13]

$$\mathcal{F}_\phi = -\frac{\Phi_E}{\tilde{\Omega}}, \qquad \mathcal{F}_r = \mathcal{F}_\phi \frac{p_r}{p_\phi}, \tag{9}$$

where $\tilde{\Omega} \equiv \dot{\phi}$ is the (dimensionless) orbital frequency, and Φ_E is the energy flux for quasi-circular orbits, which can be written as

$$\Phi_E = \frac{\tilde{\Omega}^2}{16\pi}\sum_{l=2}^{8}\sum_{m=-l}^{l} m^2 |d_L h_{lm}|^2, \tag{10}$$

where d_L is the luminosity distance of the BBH to the observer, and h_{lm} are the waveform modes.

Additionally, we use PN-expanded evolution equations for the spins and angular momentum given by

$$\frac{d\boldsymbol{S}_{\rm i}}{dT} = \boldsymbol{\Omega}_{S_{\rm i}} \times \boldsymbol{S}_{\rm i}, \tag{11a}$$

$$\boldsymbol{L} = \boldsymbol{L}(\boldsymbol{l}_N, \Omega_{\rm PN}, \boldsymbol{S}_{\rm i}), \tag{11b}$$

$$\dot{\boldsymbol{l}}_N = \dot{\boldsymbol{l}}_N(\boldsymbol{l}_N, \Omega_{\rm PN}, \boldsymbol{S}_{\rm i}), \tag{11c}$$

where $\Omega_{\rm PN}$ is the PN-expanded orbital frequency (see below), $\boldsymbol{\Omega}_{S_{\rm i}}$ is the spin-precession frequency, and $\boldsymbol{l}_N$ is the unit vector in the direction of $\boldsymbol{L}_N$. We derived these PN-expanded equations in Ref. [12] (consistently, from the `SEOBNRv5` Hamiltonian and equations of motion) for precessing spins through an orbit-averaged procedure up to 4PN, including spin-orbit (SO) contributions to next-to-next-to-leading order (NNLO), and spin-spin (SS) contributions to NNLO. We note that the SO and LO SS parts of the spin-precession frequency $\boldsymbol{\Omega}_{S_{\rm i}}$ agree with the orbit-averaged results given by Eqs. (1)-(5) of Refs. [25, 26], but the NLO and NNLO SS terms do not agree with Refs. [26, 27] because of the different gauge used for the `SEOBNRv5` Hamiltonian. Furthermore, our expressions for $\boldsymbol{L}(\boldsymbol{l}_N, \Omega_{\rm PN}, \boldsymbol{S}_{\rm i})$, and hence for $\dot{\boldsymbol{l}}_N$, differ at SO level from Ref. [25] because of using a different spin-supplementary condition.

To solve the equations of motion, we first perform the PN-expanded evolution of the spin and angular momentum vectors using Eqs. (11), then we apply a subsequent non-precessing EOB evolution where the values of $\boldsymbol{S}_{1,2}$, $\boldsymbol{l}_N$ and $\boldsymbol{L}(\boldsymbol{l}_N)$ are employed when computing the right-hand sides of the EOB equations (8) at every timestep.

The solution of the PN-expanded equations (11) requires a prescription for the evolution of the orbital frequency, which we compute using the following equation

$$\dot{\Omega}_{\rm PN} = \left[\frac{-\Phi_E}{dE/d\Omega}\right]_{\rm PN-expanded}, \tag{12}$$

where in the right-hand side we use the circular-orbit PN-expanded energy flux and the derivative of the PN-expanded energy. More specifically, Ref. [12] used the results of Ref. [28] to obtain the NNLO SS contribution to the orbit-averaged energy flux, and the PN-expanded binding energy $E(\omega)$ using the `SEOBNRv5` Hamiltonian. Our result for $\dot{\Omega}_{\rm PN}$ agrees at the NNLO SO and LO SS with Eq. (A1) of Ref. [29], but differs from it by including the NLO and NNLO SS contributions.

Our approach is similar to that of Refs. [25, 30, 31], but we include higher PN orders, and derive the PN equations from the EOB Hamiltonian employing a different gauge and spin-supplementary condition, which leads to some differences compared to previous results in the literature.

II. EFFECTIVE-ONE-BODY MULTIPOLAR WAVEFORMS FOR SPIN-PRECESSING BINARY BLACK HOLES

We briefly review the main ideas and building blocks of the EOB approach to generate waveforms for spin-precessing systems containing multipoles beyond the quadrupolar one. Here we closely follow the previous model developed in [6] (`SEOBNRv4PHM`), highlighting any differences.

A. Inspiral-plunge waveforms

The construction of the inspiral-plunge waveforms follows a similar approach to [6], with the usage of the factorized, resummed version [14, 32] of the frequency domain PN formulas of the modes [33, 34]. The factorized resummation has been developed for non-precessing BBHs [12, 15, 24, 32] and it has been proven to improve the accuracy of the PN expressions in the test-particle limit [35–38].

The components of the radiation-reaction force, $\mathcal{F}_{r,\phi}$, in Eq. (9) depend on the amplitude of the individual GW modes $|h_{lm}|$, which in the non-precessing case, are functions of $\boldsymbol{\chi}_{1,2}\cdot\boldsymbol{l}$, where $\boldsymbol{l}$ is a unit vector in the direction of $\boldsymbol{L}$. In the precessing case, these modes have an additional time dependence on the spins due to the evolution of $\boldsymbol{\chi}_{1,2}\cdot\boldsymbol{l}$. In the previous model, the spins entering the GW energy flux were projected using $\boldsymbol{l}$; however, in `SEOBNRv5PHM` we use the projections onto the Newtonian orbital angular momentum, $\boldsymbol{\chi}_{1,2}\cdot\boldsymbol{l}_N$, since $\boldsymbol{l}_N$ represents the direction perpendicular to the orbital plane (see Fig. 1) and is provided by the PN spin-precessing evolution equations.

The GW polarizations in the inertial-frame of the observer are required for data analysis studies. As in [6], the SEOBNRv5PHM model also defines three reference frames: 1) the inertial frame of the observer (*source frame*) (these quantities are indicated with a superscript I), 2) an inertial frame where the z-axis is aligned with the final angular momentum of the system[1] ($\boldsymbol{J}_{\rm f}$-*frame*), which helps with the construction of the merger ringdown, (these quantities are denoted with the superscript J), and finally 3) a non-inertial frame which tracks the instantaneous motion of the orbital plane, the *co-precessing frame* (these quantities are denoted by the superscript P). The frames are depicted in Fig. 1 and described below.

The source frame is defined at a given reference frequency $f_{\rm ref}$ (corresponding to a reference time $t_{\rm ref}$) by the triad $\{\hat{\boldsymbol{e}}^I_i\}$ $(i=1,2,3)$, where $\hat{\boldsymbol{e}}^I_1=\hat{\boldsymbol{n}}(t_{\rm ref})$, $\hat{\boldsymbol{e}}^I_3=\boldsymbol{l}_N(t_{\rm ref})$, $\hat{\boldsymbol{e}}^I_2=\hat{\boldsymbol{e}}^I_3\times\hat{\boldsymbol{e}}^I_1$. Meanwhile, the $\hat{\boldsymbol{J}}_{\rm f}$-frame is constructed as $\hat{\boldsymbol{e}}^J_3=\hat{\boldsymbol{J}}_{\rm f}$, $\hat{\boldsymbol{e}}^J_1=N[\hat{\boldsymbol{e}}^I_1-(\hat{\boldsymbol{e}}^I_1\cdot\hat{\boldsymbol{e}}^J_3)\hat{\boldsymbol{e}}^J_3]$, $\hat{\boldsymbol{e}}^J_2=\hat{\boldsymbol{e}}^J_3\times\hat{\boldsymbol{e}}^J_1$ where the $N[]$ denotes normalization. The two frames are connected by a constant rotation given by:

$$\mathbf{R}^{I\to J}=\begin{pmatrix}\hat{\boldsymbol{e}}^J_1\cdot\hat{\boldsymbol{e}}^I_1 & \hat{\boldsymbol{e}}^J_2\cdot\hat{\boldsymbol{e}}^I_1 & \hat{\boldsymbol{e}}^J_3\cdot\hat{\boldsymbol{e}}^I_1\\ \hat{\boldsymbol{e}}^J_1\cdot\hat{\boldsymbol{e}}^I_2 & \hat{\boldsymbol{e}}^J_2\cdot\hat{\boldsymbol{e}}^I_2 & \hat{\boldsymbol{e}}^J_3\cdot\hat{\boldsymbol{e}}^I_2\\ \hat{\boldsymbol{e}}^J_1\cdot\hat{\boldsymbol{e}}^I_3 & \hat{\boldsymbol{e}}^J_2\cdot\hat{\boldsymbol{e}}^I_3 & \hat{\boldsymbol{e}}^J_3\cdot\hat{\boldsymbol{e}}^I_2\end{pmatrix}. \tag{13}$$

The rotation operation in Eq. (13) can be also expressed as a unit quaternion $q_{I\to J}$[2].

Finally, to construct the inertial GW modes h^I_{lm} during the inspiral-plunge, we introduce the *co-precessing frame*, which is defined by the triad $\{\hat{\boldsymbol{e}}^P_i\}$ $(i=1,2,3)$. At every instant the z-axis of the co-precessing frame is aligned with $\boldsymbol{l}_N$; i.e., $\hat{\boldsymbol{e}}^P_3(t)=\boldsymbol{l}_N(t)$ [3]. In this frame, the GW radiation resembles the radiation from an aligned-spin binary [17–21]. The other two axes lie in the orbital plane and are defined such that they minimize precessional effects in the modes h^P_{lm}. This is done by enforcing the minimal rotation condition that relates the rotation from the $\boldsymbol{J}_{\rm f}$ final frame to the co-precessing frame. [19] This transformation is best parametrized by a unit quaternion that aligns the z-axis of the J frame with $\boldsymbol{l}_N$

$$q_{J\to P}(t)=\sqrt{-\boldsymbol{l}_N(t)\hat{\boldsymbol{e}}^J_3} \tag{14}$$

and the minimal rotation condition is then simply $(\dot{q}\hat{\boldsymbol{e}}^J_3\bar{q})_0=0$, where $(p)_0$ denotes taking the scalar part of the quaternion [19] and $\bar{q}$ denotes the conjugate of the quaternion (which is also its inverse). The minimal rotation condition has a residual freedom which corresponds to the integration constant [19]. We fix this freedom by demanding that at the reference time, the co-precessing frame and source frame coincide.

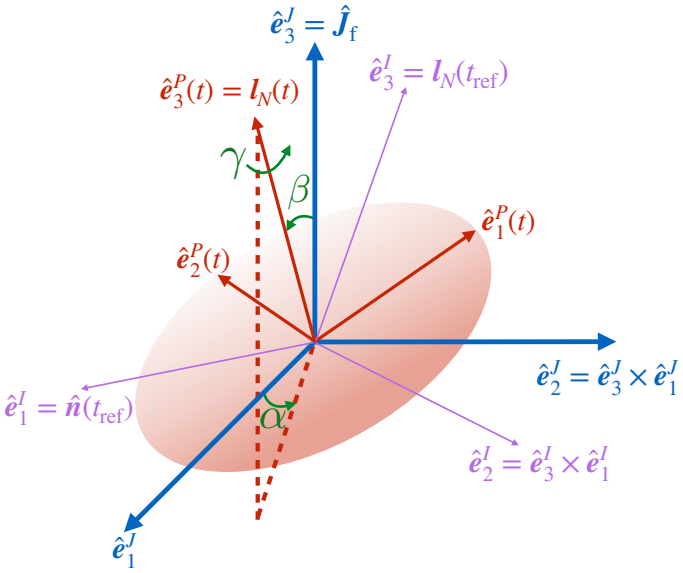

Figure 1. Frames used in the construction of the SEOBNRv5PHM model. The co-precessing frame (red) is constructed such that its z-axis is instantaneously aligned with the Newtonian angular momentum $\boldsymbol{l}_N(t)$ and can described by the Euler angles (α,β,γ) with respect to $\boldsymbol{J}_{\rm f}$-frame (blue), while the source frame (purple) corresponds to the inertial frame defined by the initial Newtonian angular momentum $\boldsymbol{l}_N(t_{\rm ref})$ and unit separation vector $\hat{\boldsymbol{n}}(t_{\rm ref})$. At $t_{\rm ref}$, the source and co-precessing frames coincide.

We calculate the co-precessing frame inspiral-plunge GW waveform modes by evaluating the factorized, resummed non-precessing modes along the EOB dynamics described in Eqs. (8), with time-dependent projections of the spins $\boldsymbol{\chi}_{1,2}\cdot\{\boldsymbol{l}_N,\boldsymbol{l}\}$. Following [22], in which an EOB non-precessing multipolar waveform (SEOBNRv5HM) calibrated to NR non-precessing simulations was developed, we include in the co-precessing frame of the SEOBNRv5PHM model the $\{(2,\pm2),(2,\pm1),(3,\pm3),(3,\pm2),(4,\pm4),(4,\pm3),(5,\pm5)\}$ modes, and make the assumption $h^P_{l,-m}=(-1)^l h^{P*}_{l,m}$. As discussed in Sec. IIIB of [6], the inaccuracies due to neglecting mode asymmetries should remain modest, and are expected to be at most comparable to other modelling errors.

To assemble the inertial frame modes, we first rotate $h^P_{\ell m}$ to $\hat{\boldsymbol{J}}_{\rm f}$-frame using $\bar{q}_{J\to P}$, and then from J-frame to the source frame using $\bar{q}_{I\to J}$ [4]. To make contact with literature, it is useful to express these rotations in terms of Euler angles. Using the active ZYZ convention (see Fig. 1), the $J\to P$ rotation is given by

$$q_{J\to P}=e^{\alpha\hat{\boldsymbol{z}}/2}e^{\beta\hat{\boldsymbol{y}}/2}e^{\gamma\hat{\boldsymbol{z}}/2} \tag{15}$$

In this formulation, the minimal rotation condition is given by $\dot{\gamma}=-\dot{\alpha}\cos\beta$.

[1] This is computed as the value of the solution of Eqs. (11) at the attachment point of the merger-ringdown model.

[2] To perform such a conversion, as well as subsequent manipulations of quaternions such as the enforcement of the minimal rotation condition we work with the `quaternion` python package [**?**].

[3] Note that in [6], the z-axis is aligned with $\boldsymbol{l}$ instead of $\boldsymbol{l}_N$.

[4] We perform these rotations using the `scri`[39–41] python package.

B. Merger-ringdown waveforms

After the coalescence, the description of a BBH system of two individual objects is no longer valid, and the EOB model builds the ringdown stage via a phenomenological model of the quasinormal modes (QNMs) of the remnant BHs, formed after the merger of the progenitors. The QNMs frequencies are tabulated functions of the final mass, M_f, and angular momentum $\boldsymbol{S}_f = M_f^2 \boldsymbol{\chi}_f$ of the remnant BH [42]. The QNMs are defined with respect to the direction of the final spin, and thus, the description of the ringdown signal as a linear combination of QNMs, is formally valid only in an inertial frame with the z-axis parallel to $\boldsymbol{\chi}_f$.

Following [6], in `SEOBNRv5PHM` the attachment of the merger-rindown waveform, each GW mode $h_{lm}^{\rm merger-RD}$, is performed in the co-precessing frame. Therefore, we employ the merger-ringdown multipolar model developed for the non-precessing BBHs (`SEOBNRv5HM`) in [22].

The calculation of the waveform in the inertial observer's frame requires a description of the co-precessing frame Euler angles $\{\alpha(t),\beta(t),\gamma(t)\}$ which extends beyond merger. Here, we follow a similar approach as in the `SEOBNRv4PHM`, and take advantage from a phenomenological prescription based on insights from NR simulations [43]. Precisely, it was shown that the co-precessing frame continues to precess roughly around the direction of the final angular momentum with a precession frequency, $\omega_{\rm prec}$, proportional to the difference between the lowest overtone of the $(2,2)$ and $(2,1)$ QNM frequencies, while the opening angle of the precessing cone, β, tends to decrease at merger. These phenomenology translates into the following expressions for the merger-ringdown angles in `SEOBNRv5PHM`,

$$\alpha^{\rm merger-RD} = \alpha(t_{\rm attach}) + \omega_{\rm prec}(t - t_{\rm attach}), \tag{16}$$

$$\beta^{\rm merger-RD} = \beta(t_{\rm attach}), \tag{17}$$

$$\gamma^{\rm merger-RD} = \gamma(t_{\rm attach}) - \cos(\omega_{\rm prec}(t - t_{\rm attach})), \tag{18}$$

where $t_{\rm attach}$ is the time of attachment of the merger-ringdown model. We have also investigated non-constant post-merger extensions of the β angle, such as the small opening angle approximation (see Eq. (24b) of [44]), but we find that such an approximation may degrade the faithfulness of the model to NR for certain configurations.

The behavior noticed in [43] describes prograde configurations, were the remnant spin is positively aligned with the orbital angular momentum at merger. However, to keep the model generic and accurate in a wide parameter space of mass ratios and spins, we extend the prescription to the retrograde case (negative alignment of the final spin with respect to the angular momentum at merger), which is typical for high mass ratio binaries, when the total angular momentum $\boldsymbol{J}$ is dominated by the primary spin $\boldsymbol{S}_1$ instead of $\boldsymbol{L}$. While keeping imposing simple precession around the final spin at a rate $\omega_{\rm prec} \geq 0$ in our model, we distinguish two cases depending on the direction of the total angular momentum at merger $\boldsymbol{\chi}_f \sim \boldsymbol{J}_{\rm merger}$ with respect to the final orbital angular momentum $\boldsymbol{L}_f$,

$$\omega_{\rm prec} = \begin{cases} \omega_{22}^{\rm QNM}(\chi_f) - \omega_{21}^{\rm QNM}(\chi_f) & \text{if} \quad \boldsymbol{\chi}_f \cdot \boldsymbol{L}_f > 0 \\ \omega_{2-1}^{\rm QNM}(\chi_f) - \omega_{2-2}^{\rm QNM}(\chi_f) & \text{if} \quad \boldsymbol{\chi}_f \cdot \boldsymbol{L}_f < 0 \end{cases}, \tag{19}$$

where $\chi_f = |\boldsymbol{\chi}_f|$, and the QNM frequencies for negative m are taken from the continous extension of the $m > 0$, $\omega_{lm}^{\rm QNM} > 0$ branch [42]. We stress that this prescription of the post-merger extension of the Euler angles for the retrograde case is much less tested than the prograde case due to the lack of NR simulations covering this region of parameter space, which also includes particular systems with transitional precession [45].

Following recent insights from NR of [46], where a correct prescription of the shift of the co-precessing quasi-normal mode frequencies was developed, we compute in the `SEOBNRv5PHM` model the co-precessing frame quasi-normal mode frequencies from the quasi-normal mode frequencies in the J-frame as,

$$\omega_{lm}^{\rm QNM,P} = \omega_{lm}^{\rm QNM,J} - m(1 - |\cos\beta_{\rm attach}|)\omega_{\rm prec}. \tag{20}$$

Another essential aspect in the construction of the merger-rindown waveforms is the mapping from binary components masses and spins to the final mass and spin, required to evaluate the QNM frequencies of the remnant. Several groups have developed fitting formulas based on large sets of NR simulations (see [47] for a brief overview of the literature). To ensure agreement in the non-precessing limit with `SEOBNRv5HM` [22], we employ the fits for the final mass from Jiménez-Forteza et al. [48], and the fits from Hofmann et al [49] for the final spin.

The application of the fitting formulae for the final mass and spin requires choosing a time during the inspiral at which to evaluate the spins, as for precessing binaries the individual components of the spins vary with time. In the `SEOBNRv5PHM` model, we choose to evaluate the spins at a time corresponding to an orbital separation $r = 10M$. Similarly as in [6], this choice is based on good agreement with NR configurations, and by the restriction that the smallest initial orbital separation must be $r > 10.5M$ to ensure small initial eccentricities [5]. Additionally, this choice guarantees that a given physical configuration will always produce the same waveform regardless of the initial starting frequency, as all configurations will pass through an orbital separation $r = 10M$.

Finally, the inspiral-merger-ringdown GW modes in the inertial frame h_{lm}^I are obtained by rotating the inspiral-merger-ringdown modes h_{lm}^P from the co-precessing frame to the inertial observer's frame using the expressions for the rotations in Appendix A of [5]. The inertial frame GW polarizations at a time t, and location in the sky of the observer (φ_0, ι) can be expressed in terms of the -2-spin-weighted spherical harmonics, as follows

$$h_+^{\rm I}(t;\boldsymbol{\lambda},\varphi_0,\iota) - i h_\times^{\rm I}(t;\boldsymbol{\lambda},\varphi_0,\iota) = \sum_{\ell,m} {}_{-2}Y_{\ell m}(\varphi_0,\iota)\, h_{\ell m}^{\rm I}(t;\boldsymbol{\lambda}), \tag{21}$$

where $\boldsymbol{\lambda}$ represents the set of intrinsic parameters, and $\{\varphi_0, \iota\}$ the coalescence phase and the inclination angle of the signal.

For applications in which only the polarizations are required, as for most of the current parameter estimation codes,

we introduce an alternative and computationally more efficient method to obtain the polarizations directly in terms the co-precessing spin-weighted spherical harmonic modes, i.e., rotating the spin-weighted spherical harmonic basis, instead of computing the full set of spin-weighted spherical harmonic modes in the inertial frame.

The inertial-frame (*I-frame*) modes are related to the co-precessing-frame (*P-frame*) modes by a time-dependent rotation from the co-precessing frame to the frame where the z-axis is aligned with the final angular momentum of the system (***J***-*frame*[5]) and a time-independent rotation from the ***J***-frame to the final inertial frame

$$h^{\rm I}_{\ell m}(t) = \sum_{m',m''} \left(\mathbf{R}^{\rm J\to I}\right)_{m,m'} \left(\mathbf{R}^{\rm P\to J}\right)_{m',m''} h^{\rm P}_{\ell m''}(t), \tag{22}$$

where $\mathbf{R}^{\rm X\to Y}$ indicates the rotation operator from the frame X to the frame Y, and the indices m',m'' indicate summation over modes available in the co-precessing frame.

Factoring out the source orientation information from the spin-weighted spherical harmonic basis as a rotation of the basis

$${}_{-2}Y_{\ell m}(\varphi_0,\iota) = \sum_{m'} \left(\mathbf{R}^{\varphi_0,\iota}\right)_{m,m'} {}_{-2}Y_{\ell m}(0,0), \tag{23}$$

the complete rotation of the basis functions from the co-precessing frame to the final inertial frame can be constructed composing the individual rotations as

$$\mathbf{R}^{\rm P\to I} = \mathbf{R}^{\varphi_0,\iota}\mathbf{R}^{\rm J\to I}\mathbf{R}^{\rm P\to J}, \tag{24}$$

with associated Euler angles $\{\alpha_{\rm P\to I},\beta_{\rm P\to I},\gamma_{\rm P\to I}\}$. Applying this rotation operator, the spin-weighted spherical harmonic basis can be written as

$$\sum_{m'} \left(\mathbf{R}^{\rm P\to I}\right)_{m,m'} {}_{-2}Y_{\ell m}(0,0) = e^{2i\alpha_{\rm P\to I}} {}_{-2}Y_{\ell m}(\gamma_{\rm P\to I},\beta_{\rm P\to I}), \tag{25}$$

and the GW polarizations in the inertial frame can therefore be expressed as

$$h^{\rm I}_{+}(\varphi_0,\iota;t) - i h^{\rm I}_{\times}(\varphi_0,\iota;t) = e^{2i\alpha_{\rm P\to I}} \sum_{\ell,m} {}_{-2}Y_{\ell m}(\gamma_{\rm P\to I},\beta_{\rm P\to I}) h^{\rm P}_{\ell m}(t). \tag{26}$$

Eq. (26) is only summed over the set of 7 co-precessing modes[6], and the computation of the complete rotation and its application to the basis functions is more efficient than the corresponding (double) rotation of the GW modes, which implies the rotation of 33 GW modes.

III. PRECESSING-SPIN HAMILTONIAN

In this Appendix, we write the precessing-spin Hamiltonian derived in Ref. [12], which reduces to the Hamiltonian of `SEOBNRv5HM` [22] in the aligned-spin limit, and includes in-plane spin components in an orbit average for circular orbits.

The effective Hamiltonian is given by

$$\begin{aligned}\tilde{H}_{\rm eff} = &\frac{1}{r^3 + a_+^2(r+2)}\left[\tilde{\boldsymbol{L}}\cdot(g_{a_+}\boldsymbol{a}_+ + g_{a_-}\delta\boldsymbol{a}_-) + {\rm SO}_{\rm calib} + G_{a^3}\right] \\ &+ \left[A\left(1 + B_p\frac{\tilde{L}^2}{r^2} + (1+B_{np})p_r^2 + B_{npa}\frac{(\tilde{\boldsymbol{L}}\cdot\boldsymbol{a}_+)^2}{r^2} + Q\right)\right]^{1/2},\end{aligned} \tag{27}$$

where the gyro-gravitomagnetic factors are the same as in the aligned-spin case, which are given by Eq. (28) of Ref. [12], and the SO calibration term is given by

$${\rm SO}_{\rm calib} = d_{\rm SO}\frac{\nu}{r^3}\tilde{\boldsymbol{L}}\cdot\boldsymbol{a}_+. \tag{28}$$

with the same value of $d_{\rm SO}$ as the aligned-spin model [22]. The cubic-in-spin term G_{a^3} reads

$$\begin{aligned}G_{a^3} = &\delta\tilde{\boldsymbol{L}}\cdot\boldsymbol{a}_-\left\{\frac{1}{r^2}\left[\frac{a_+^2}{24} + \frac{5}{24}\left(a_+^2 - (\boldsymbol{l}_N\cdot\boldsymbol{a}_+)^2\right)\right]\right. \\ &\left. - \frac{\tilde{L}^2}{8r^3}\left(a_+^2 - (\boldsymbol{l}_N\cdot\boldsymbol{a}_+)^2\right)\right\} \\ &+ \tilde{\boldsymbol{L}}\cdot\boldsymbol{a}_+\left\{\frac{\tilde{L}^2}{r^3}\left[\frac{\delta}{4}\left[\boldsymbol{a}_+\cdot\boldsymbol{a}_- - (\boldsymbol{l}_N\cdot\boldsymbol{a}_+)(\boldsymbol{l}_N\cdot\boldsymbol{a}_-)\right]\right.\right. \\ &\left. - \frac{1}{8}\left(a_+^2 - (\boldsymbol{l}_N\cdot\boldsymbol{a}_+)^2\right)\right] \\ &+ \frac{1}{r^2}\left[-\frac{a_+^2}{4} - \frac{3}{8}\left(a_+^2 - (\boldsymbol{l}_N\cdot\boldsymbol{a}_+)^2\right) + \delta\frac{5}{24}(\boldsymbol{a}_+\cdot\boldsymbol{a}_-)\right. \\ &\left.\left. - \delta\frac{5}{6}\left[\boldsymbol{a}_+\cdot\boldsymbol{a}_- - (\boldsymbol{l}_N\cdot\boldsymbol{a}_+)(\boldsymbol{l}_N\cdot\boldsymbol{a}_-)\right]\right]\right\}.\end{aligned} \tag{29}$$

The coefficients A, B_p, B_{np}, B_{npa}, and Q include nonspinning and SS PN terms, such that

$$\begin{aligned}A &= \frac{a_+^2u^2 + A_{\rm pm} + A^{\rm align}_{\rm SS} + A^{\rm prec}_{\rm SS}}{1 + a_+^2u^2(2u+1)}, \\ B_p &= 1 + B^{\rm prec}_{p,\rm SS}, \\ B_{np} &= -1 + a_+^2u^2 + A_{\rm pm}\bar{D}_{\rm pm} + B^{\rm align}_{np,\rm SS}, \\ B_{npa} &= -\frac{(1+2u)u^2}{1 + a_+^2u^2(1+2u)}, \\ Q &= Q_{\rm pm} + Q^{\rm align}_{\rm SS},\end{aligned} \tag{30}$$

where the nonspinning contributions $A_{\rm pm}$, $\bar{D}_{\rm pm}$ and $Q_{\rm pm}$ are given by Eqs. (20)–(23) of Ref. [12], while the SS corrections read

$$A_{\rm SS}^{\rm align} = \frac{1}{r^4}\left[\frac{9a_+^2}{8} - \frac{5}{4}\delta\boldsymbol{a}_-\cdot\boldsymbol{a}_+ + a_-^2\left(\frac{\nu}{2}+\frac{1}{8}\right)\right] + \frac{1}{r^5}\left[a_+^2\left(-\frac{175\nu}{64}-\frac{225}{64}\right) + \delta\boldsymbol{a}_-\cdot\boldsymbol{a}_+\left(\frac{117}{32}-\frac{39\nu}{16}\right) + a_-^2\left(\frac{21\nu^2}{16}-\frac{81\nu}{64}-\frac{9}{64}\right)\right], \tag{31a}$$

$$B_{np,\rm SS}^{\rm align} = \frac{1}{r^3}\left[a_+^2\left(3\nu+\frac{45}{16}\right) - \frac{21}{8}\delta\boldsymbol{a}_-\cdot\boldsymbol{a}_+ + a_-^2\left(\frac{3\nu}{4}-\frac{3}{16}\right)\right] + \frac{1}{r^4}\left[a_+^2\left(-\frac{1171\nu}{64}-\frac{861}{64}\right) + \delta\boldsymbol{a}_-\cdot\boldsymbol{a}_+\left(\frac{13\nu}{16}+\frac{449}{32}\right) + a_-^2\left(\frac{\nu^2}{16}+\frac{115\nu}{64}-\frac{37}{64}\right)\right], \tag{31b}$$

$$Q_{\rm SS}^{\rm align} = \frac{p_r^4}{r^3}\left[a_+^2\left(-5\nu^2+\frac{165\nu}{32}+\frac{25}{32}\right) + \delta\boldsymbol{a}_-\cdot\boldsymbol{a}_+\left(\frac{45\nu}{8}-\frac{5}{16}\right) + a_-^2\left(-\frac{15\nu^2}{8}+\frac{75\nu}{32}-\frac{15}{32}\right)\right], \tag{31c}$$

$$A_{\rm SS}^{\rm prec} = \frac{a_+^2-(\boldsymbol{l}_N\cdot\boldsymbol{a}_+)^2}{r^3} + \frac{1}{r^4}\left\{\frac{33}{16}\delta\left[\boldsymbol{a}_+\cdot\boldsymbol{a}_- - (\boldsymbol{l}_N\cdot\boldsymbol{a}_+)(\boldsymbol{l}_N\cdot\boldsymbol{a}_-)\right] + \left(-\frac{\nu}{4}-\frac{3}{16}\right)\left[a_-^2-(\boldsymbol{l}_N\cdot\boldsymbol{a}_-)^2\right] + \left(\frac{7\nu}{8}-\frac{31}{8}\right)\left[a_+^2-(\boldsymbol{l}_N\cdot\boldsymbol{a}_+)^2\right]\right\} + \frac{1}{r^5}\left\{\delta\left(\frac{17}{2}\nu-\frac{1}{8}\right)\left[\boldsymbol{a}_+\cdot\boldsymbol{a}_- - (\boldsymbol{l}_N\cdot\boldsymbol{a}_+)(\boldsymbol{l}_N\cdot\boldsymbol{a}_-)\right] + \left(-\frac{41\nu^2}{16}+\frac{583\nu}{64}-\frac{171}{128}\right)\left[a_-^2-(\boldsymbol{l}_N\cdot\boldsymbol{a}_-)^2\right] + \left(-\frac{11\nu^2}{16}+\frac{1435\nu}{192}+\frac{187}{128}\right)\left[a_+^2-(\boldsymbol{l}_N\cdot\boldsymbol{a}_+)^2\right]\right\}, \tag{31d}$$

$$B_{p,\rm SS}^{\rm prec} = -\frac{a_+^2-(\boldsymbol{l}_N\cdot\boldsymbol{a}_+)^2}{2r^2} + \frac{1}{r^3}\left\{\frac{3}{8}\delta\left[\boldsymbol{a}_+\cdot\boldsymbol{a}_- - (\boldsymbol{l}_N\cdot\boldsymbol{a}_+)(\boldsymbol{l}_N\cdot\boldsymbol{a}_-)\right] + \left(\frac{3}{32}-\frac{3\nu}{8}\right)\left[a_-^2-(\boldsymbol{l}_N\cdot\boldsymbol{a}_-)^2\right] + \left(-\frac{7\nu}{8}-\frac{15}{32}\right)\left[a_+^2-(\boldsymbol{l}_N\cdot\boldsymbol{a}_+)^2\right]\right\} + \frac{1}{r^4}\left\{\delta\left(-\frac{49\nu}{8}-\frac{43}{16}\right)\left[\boldsymbol{a}_+\cdot\boldsymbol{a}_- - (\boldsymbol{l}_N\cdot\boldsymbol{a}_+)(\boldsymbol{l}_N\cdot\boldsymbol{a}_-)\right] + \left(\frac{19\nu^2}{16}-\frac{545\nu}{64}+\frac{219}{128}\right)\left[a_-^2-(\boldsymbol{l}_N\cdot\boldsymbol{a}_-)^2\right] + \left(\frac{11\nu^2}{16}-\frac{805\nu}{192}+\frac{125}{128}\right)\left[a_+^2-(\boldsymbol{l}_N\cdot\boldsymbol{a}_+)^2\right]\right\}, \tag{31e}$$

where $A_{\rm SS}^{\rm prec}$ and $B_{p,\rm SS}^{\rm prec}$ only contain in-plane spin components that were orbit-averaged using

$$\begin{aligned}\langle(\boldsymbol{n}\cdot\boldsymbol{a}_+)^2\rangle &= \frac{1}{2}\left[a_+^2-(\boldsymbol{l}_N\cdot\boldsymbol{a}_+)^2\right],\\ \langle(\boldsymbol{n}\cdot\boldsymbol{a}_-)^2\rangle &= \frac{1}{2}\left[a_-^2-(\boldsymbol{l}_N\cdot\boldsymbol{a}_-)^2\right],\\ \langle(\boldsymbol{n}\cdot\boldsymbol{a}_+)(\boldsymbol{n}\cdot\boldsymbol{a}_-)\rangle &= \frac{1}{2}\left[\boldsymbol{a}_+\cdot\boldsymbol{a}_- - (\boldsymbol{l}_N\cdot\boldsymbol{a}_+)(\boldsymbol{l}_N\cdot\boldsymbol{a}_-)\right].\end{aligned} \tag{32}$$

IV. POST-ADIABATIC DYNAMICS

Since `SEOBNRv5PHM` evolves *aligned-spin* EOB dynamics we can apply the iterative post-adiabatic approach which was pioneered in [50] and used in subsequent TEOBResumS [30] and SEOBNR models [51] (For example, the latest spin-precessing model `TEOBResumSv3` [30]) uses this approach). The crucial difference with the aligned-spin case is that one must vary the spins that enter the Hamiltonian and the flux at different points in the radial grid. Following the procedure outlined in Ref. [50], we obtain the following explicit equations for the corrections to the momenta:

$$p_{r_*} = \frac{\xi}{2\left(1+B_{np}\right)}\left[\mathcal{F}_\phi\left(\frac{dp_\phi}{dr}\right)^{-1}\frac{2H_{EOB}H_{\rm even}}{A} - \xi\frac{\partial Q}{\partial p_{r_*}}\right], \tag{33}$$

$$K_0 p_\phi^2 + 2H_{\rm even}\frac{\partial\bar{H}_{\rm odd}}{\partial r}p_\phi + K_1 + \frac{2H_{\rm even}H_{EOB}}{\xi}\left(\frac{dp_{r_*}}{dr}\frac{dr}{dt} - \frac{p_{r_*}}{p_\phi}\mathcal{F}_\phi\right) = 0, \tag{34}$$

where we split the effective Hamiltonian into odd and even-in-spin parts, i.e. $H_{\rm eff} \equiv H_{\rm odd} + H_{\rm even}$, defined $\bar{H}_{\rm odd} \equiv H_{\rm odd}/p_\phi$ and

[5] The $\boldsymbol{J}$-frame is the frame where the approximation of the Euler angles in Eq. (19) is applied.

[6] The negative m modes in the co-precessing frame are obtained by the symmetry relation $h^P_{l,-m} = (-1)^l h^{P*}_{l,m}$.

$$
\begin{aligned}
K_0 &\equiv \frac{dA}{dr}\left(\frac{B_p}{r^2}+\frac{(\boldsymbol{l}\cdot\boldsymbol{a}_+)^2}{r^2}B_{npa}\right)+A\left(-\frac{2}{r^3}\left(B_p+B_{npa}\frac{(\boldsymbol{l}\cdot\boldsymbol{a}_+)^2}{r^2}\right)+\frac{(\boldsymbol{l}\cdot\boldsymbol{a}_+)^2}{r^2}\frac{dB_{npa}}{dr}+\frac{1}{r^2}\frac{dB_p}{dr}\right),\\
K_1 &\equiv \frac{dA}{dr}\left(\mu^2+\frac{p_{r_*}^2}{\xi^2}\left(1+B_{np}\right)+Q\right)+A\left(\frac{p_{r_*}^2}{\xi^2}\left[\frac{dB_{np}}{dr}-\frac{2}{\xi}\frac{d\xi}{dr}\left(1+B_{np}\right)\right]+\frac{\partial Q}{\partial r}\right)
\end{aligned}
\tag{35}
$$

[1] A. Buonanno and T. Damour, Phys. Rev. D **59**, 084006 (1999), arXiv:gr-qc/9811091.
[2] A. Buonanno and T. Damour, Phys. Rev. D **62**, 064015 (2000), arXiv:gr-qc/0001013.
[3] T. Damour, Phys. Rev. D **64**, 124013 (2001), arXiv:gr-qc/0103018.
[4] Y. Pan, A. Buonanno, A. Taracchini, L. E. Kidder, A. H. Mroué, H. P. Pfeiffer, M. A. Scheel, and B. Szilágyi, Phys. Rev. D **89**, 084006 (2014), arXiv:1307.6232 [gr-qc].
[5] S. Babak, A. Taracchini, and A. Buonanno, Phys. Rev. D **95**, 024010 (2017), arXiv:1607.05661 [gr-qc].
[6] S. Ossokine *et al.*, Phys. Rev. D **102**, 044055 (2020), arXiv:2004.09442 [gr-qc].
[7] T. Hinderer and S. Babak, Phys. Rev. D **96**, 104048 (2017), arXiv:1707.08426 [gr-qc].
[8] M. Khalil, A. Buonanno, J. Steinhoff, and J. Vines, Phys. Rev. D **104**, 024046 (2021), arXiv:2104.11705 [gr-qc].
[9] A. Ramos-Buades, A. Buonanno, M. Khalil, and S. Ossokine, Phys. Rev. D **105**, 044035 (2022), arXiv:2112.06952 [gr-qc].
[10] E. Barausse, E. Racine, and A. Buonanno, Phys. Rev. D **80**, 104025 (2009), [Erratum: Phys.Rev.D 85, 069904 (2012)], arXiv:0907.4745 [gr-qc].
[11] E. Barausse and A. Buonanno, Phys. Rev. D **81**, 084024 (2010), arXiv:0912.3517 [gr-qc].
[12] M. Khalil *et al.*, in preparation (2022).
[13] A. Buonanno, Y. Chen, and T. Damour, Phys. Rev. D **74**, 104005 (2006), arXiv:gr-qc/0508067.
[14] T. Damour and A. Nagar, Phys. Rev. D **76**, 064028 (2007), arXiv:0705.2519 [gr-qc].
[15] T. Damour, B. R. Iyer, and A. Nagar, Phys. Rev. D **79**, 064004 (2009), arXiv:0811.2069 [gr-qc].
[16] T. D. Knowles, C. Devine, D. A. Buch, S. A. Bilgili, T. R. Adams, Z. B. Etienne, and S. T. Mcwilliams, Class. Quant. Grav. **35**, 155003 (2018), arXiv:1803.06346 [gr-qc].
[17] A. Buonanno, Y.-b. Chen, and M. Vallisneri, Phys. Rev. D **67**, 104025 (2003), [Erratum: Phys.Rev.D 74, 029904 (2006)], arXiv:gr-qc/0211087.
[18] P. Schmidt, M. Hannam, S. Husa, and P. Ajith, Phys. Rev. D **84**, 024046 (2011), arXiv:1012.2879 [gr-qc].
[19] M. Boyle, R. Owen, and H. P. Pfeiffer, Phys. Rev. D **84**, 124011 (2011), arXiv:1110.2965 [gr-qc].
[20] R. O'Shaughnessy, B. Vaishnav, J. Healy, Z. Meeks, and D. Shoemaker, Phys. Rev. D **84**, 124002 (2011), arXiv:1109.5224 [gr-qc].
[21] P. Schmidt, M. Hannam, and S. Husa, Phys. Rev. D **86**, 104063 (2012), arXiv:1207.3088 [gr-qc].
[22] L. Pompili *et al.*, in preparation (2022).
[23] A. Taracchini *et al.*, Phys. Rev. D **89**, 061502 (2014), arXiv:1311.2544 [gr-qc].
[24] R. Cotesta, A. Buonanno, A. Bohé, A. Taracchini, I. Hinder, and S. Ossokine, Phys. Rev. D **98**, 084028 (2018), arXiv:1803.10701 [gr-qc].
[25] S. Akcay, R. Gamba, and S. Bernuzzi, Phys. Rev. D **103**, 024014 (2021), arXiv:2005.05338 [gr-qc].
[26] Note on the derivation of the angular momentum and spin precessing equations in SpinTaylor codes. Riccardo Sturani, (https://dcc.ligo.org/DocDB/0122/T1500554/023/dLdS.pdf).
[27] A. Bohé, G. Faye, S. Marsat, and E. K. Porter, Class. Quant. Grav. **32**, 195010 (2015), arXiv:1501.01529 [gr-qc].
[28] G. Cho, R. A. Porto, and Z. Yang, (2022), arXiv:2201.05138 [gr-qc].
[29] K. Chatziioannou, A. Klein, N. Yunes, and N. Cornish, Phys. Rev. D **88**, 063011 (2013), arXiv:1307.4418 [gr-qc].
[30] R. Gamba, S. Akçay, S. Bernuzzi, and J. Williams, Phys. Rev. D **106**, 024020 (2022), arXiv:2111.03675 [gr-qc].
[31] H. Estellés, A. Ramos-Buades, S. Husa, C. García-Quirós, M. Colleoni, L. Haegel, and R. Jaume, Phys. Rev. D **103**, 124060 (2021), arXiv:2004.08302 [gr-qc].
[32] Y. Pan, A. Buonanno, R. Fujita, E. Racine, and H. Tagoshi, Phys. Rev. D **83**, 064003 (2011), [Erratum: Phys.Rev.D 87, 109901 (2013)], arXiv:1006.0431 [gr-qc].
[33] K. G. Arun, A. Buonanno, G. Faye, and E. Ochsner, Phys. Rev. D **79**, 104023 (2009), [Erratum: Phys.Rev.D 84, 049901 (2011)], arXiv:0810.5336 [gr-qc].
[34] C. K. Mishra, A. Kela, K. G. Arun, and G. Faye, Phys. Rev. D **93**, 084054 (2016), arXiv:1601.05588 [gr-qc].
[35] A. Taracchini, A. Buonanno, S. A. Hughes, and G. Khanna, Phys. Rev. D **88**, 044001 (2013), [Erratum: Phys.Rev.D 88, 109903 (2013)], arXiv:1305.2184 [gr-qc].
[36] E. Barausse, A. Buonanno, S. A. Hughes, G. Khanna, S. O'Sullivan, and Y. Pan, Phys. Rev. D **85**, 024046 (2012), arXiv:1110.3081 [gr-qc].
[37] S. Bernuzzi, A. Nagar, and A. Zenginoglu, Phys. Rev. D **84**, 084026 (2011), arXiv:1107.5402 [gr-qc].
[38] E. Harms, G. Lukes-Gerakopoulos, S. Bernuzzi, and A. Nagar, Phys. Rev. D **93**, 044015 (2016), [Addendum: Phys.Rev.D 100, 129901 (2019)], arXiv:1510.05548 [gr-qc].
[39] M. Boyle, Phys. Rev. D **87**, 104006 (2013), arXiv:1302.2919 [gr-qc].
[40] M. Boyle, L. E. Kidder, S. Ossokine, and H. P. Pfeiffer, (2014), arXiv:1409.4431 [gr-qc].
[41] M. Boyle, Phys. Rev. D **93**, 084031 (2016), arXiv:1509.00862 [gr-qc].
[42] E. Berti, V. Cardoso, and C. M. Will, Phys. Rev. D **73**, 064030 (2006), arXiv:gr-qc/0512160.
[43] R. O'Shaughnessy, L. London, J. Healy, and D. Shoemaker, Phys. Rev. D **87**, 044038 (2013), arXiv:1209.3712 [gr-qc].
[44] H. Estellés, M. Colleoni, C. García-Quirós, S. Husa, D. Keitel, M. Mateu-Lucena, M. d. L. Planas, and A. Ramos-Buades, Phys. Rev. D **105**, 084040 (2022), arXiv:2105.05872 [gr-qc].
[45] T. A. Apostolatos, C. Cutler, G. J. Sussman, and K. S. Thorne, Phys. Rev. D **49**, 6274 (1994).

[46] E. Hamilton, L. London, and M. Hannam, (2023), arXiv:2301.06558 [gr-qc].
[47] V. Varma, D. Gerosa, L. C. Stein, F. Hébert, and H. Zhang, Phys. Rev. Lett. **122**, 011101 (2019), arXiv:1809.09125 [gr-qc].
[48] X. Jiménez-Forteza, D. Keitel, S. Husa, M. Hannam, S. Khan, and M. Pürrer, Phys. Rev. D **95**, 064024 (2017), arXiv:1611.00332 [gr-qc].
[49] F. Hofmann, E. Barausse, and L. Rezzolla, Astrophys. J. Lett. **825**, L19 (2016), arXiv:1605.01938 [gr-qc].
[50] A. Nagar and P. Rettegno, Phys. Rev. D **99**, 021501 (2019), arXiv:1805.03891 [gr-qc].
[51] D. P. Mihaylov, S. Ossokine, A. Buonanno, and A. Ghosh, Phys. Rev. D **104**, 124087 (2021), arXiv:2105.06983 [gr-qc].